

Supplementary material

MXene quantum dots functionalized bimetallic MOFs as a label-free aptasensor for highly sensitive detection of exosomes

Xue Su ^{a,b}, Qiannan You ^{a*}, Panyong Wang ^{a,b}, Li Li ^{a,b}, Mingfeng Ge ^{a,b}, Li Yang ^{c,d*},
Wen-Fei Dong ^{a,b}, Zhimin Chang ^{a*}

^a Suzhou Institute of Biomedical Engineering and Technology, Chinese Academy of Science, Suzhou 215163, P. R. China

^b School of Biomedical Engineering (Suzhou), Division of Life Sciences and Medicine, University of Science and Technology of China, Hefei 230026, P. R. China

^c Chongqing Institute of Green and Intelligent Technology, Chinese Academy of Sciences, Chongqing 400714, P. R. China

^d Sansure Biotech Incorporation, Changsha, Hunan 410000, P. R. China

Corresponding Author

* E-mail: youqn@sibet.ac.cn; ylyhp@126.com; changzm@sibet.ac.cn

S1. Reagents and materials

Niobium aluminum carbide (Nb_2AlC) powder was purchased from 11 technology Co, Ltd. Hydrochloric acid (HCl) and Lithium fluoride (LiF) was obtained from Shanghai Lingfeng Chemical Reagent Co, Ltd, China and Shanghai Aladdin Biochemical Technology Co, Ltd, China, respectively. Potassium Ferricyanide ($\text{K}_3[\text{Fe}(\text{CN})_6]$), Cupric nitrate trihydrate ($\text{Cu}(\text{NO}_3)_2 \cdot 3\text{H}_2\text{O}$), Nickel nitrate hexahydrate ($\text{Ni}(\text{NO}_3)_2 \cdot 6\text{H}_2\text{O}$), N,N-dimethylformamide (DMF), Terephthalic acid, dimethyl sulfoxide (DMSO), tris (hydroxymethyl) aminomethane (Tris), ethylene diamine tetraacetic acid (EDTA), sodium hydroxide (NaOH) and sodium chloride (NaCl) were all purchased from Adamas Reagent Co., Ltd. (Shanghai, China). 1-ethyl-3-[3-(dimethylamino) propyl] carbodiimide hydrochloride (EDC) and N-hydroxysuccinimide (NHS) were obtained from Beijing Chemical Reagent Co. (Beijing China). Indium tin oxide (ITO) electrodes ($10 \text{ mm} \times 10 \text{ mm} \times 1.1 \text{ mm}$) were purchased from Zhuhai Kaivo Optoelectronic Technology Co., Ltd. (Guangdong, China). The specific aptamer sequences were synthesized by Sangong Biotech. Co., Ltd. (Shanghai, China). The sequences of the amino modified oligonucleotides were as follows:

CD63: 5'-NH₂-TTTTTTCACCCACCTCGCTCCCGTGACACTAATGCTA-3'

MUC1: 5'-NH₂-TTTTTGCAGTTGATCCTTTGGATACCCTGG-3'

To assess selectivity, a random aptamer sequence was used, and the sequence of the oligonucleotide was given as:

5'-NH₂-TTTTTTNN-3'

S2. Testing apparatus

Scanning electron microscope (SEM) results were conducted by Regulus-8100 instrument. Transmission electron microscopy (TEM) images were obtained on HITACHI H-7800 instrument and High-resolution transmission electron microscope (HRTEM) results were accomplished by a TF-G20 instrument. X-ray diffraction (XRD) patterns were gained by Bruker D8 ADVANCE and X-ray photoelectron spectroscopy (XPS) results were gained by KRATOS AXIS. Fourier transform infrared spectroscopy (FT-IR) patterns were obtained by Thermo Scientific Nicolet iS20. The

nanoparticle tracking analysis (NTA) was conducted by NanoSight NS300 instrument and negative staining electron microscopy experiment was completed by JEOL JEM-1400Plus instrument. Zeta potential measurement was administered by Zetasizer NANO ZS90 instrument.

S3. Cell culture and exosomes extraction

Non-small cell lung cancer cell line A549 cells were purchased from Shanghai Zhong Qiao Xin Zhou Biotechnology Co, Ltd. The cells were cultured in 1640 RPMI with 10% (v/v) FBS and 1% (v/v) penicillin-streptomycin in an incubator with 5% CO₂ at 37 °C. A549 cell-derived exosomes were extracted by ultracentrifugation as follows: The A549 cells were collected when they were grown to more than 80 % and incubated with a total exosome isolation kit overnight at 4 °C. Afterwards, the incubation solution was centrifuged at 10000 g for 60 min to discard the larger vesicles. Subsequently, the precipitate was washed with 0.01 M phosphate-buffered saline (PBS, PH=7.4) by ultracentrifugation at 10000 g for 60 min to obtain exosomes. The final exosomes were obtained by resuspending the precipitation with 0.01 M PBS and filtered through a 0.22 μm pore filter, then stored at - 20 °C for further use. The size, concentration, and morphology of the extracted exosomes were characterized by nanoparticle tracking analysis (NTA) and negative staining electron microscopy.

S4. Electrochemical measurements

Cyclic voltammetry (CV), differential pulse voltammetry (DPV), and electrochemical impedance spectroscopy (EIS) measurements were conducted on a CHI660E electrochemical workstation (Shanghai Chenhua Instrument Co., Ltd., China) by a three-electrode system (a working electrode, a saturated silver-silver chloride electrode (Ag/AgCl) reference electrode, and a platinum wire counter electrode). CV was conducted in 0.1 M KCl solution containing 5 mM K₃[Fe(CN)₆], with the range from -0.2 V to 0.6 V. EIS tests were performed in 0.1 M KCl solution containing 5 mM K₃[Fe(CN)₆]/K₄[Fe (CN)₆] (1:1), with an amplitude of 5 mV in a frequency range of 0.1 Hz~10 kHz. DPV test was used to compare the performance of aptasensors in detecting exosomes, which was conducted in 0.1 M KCl solution containing 5 mM K₃[Fe(CN)₆] with the range from - 0.2 V to 0.6 V. All measurements were carried out

at room temperature.

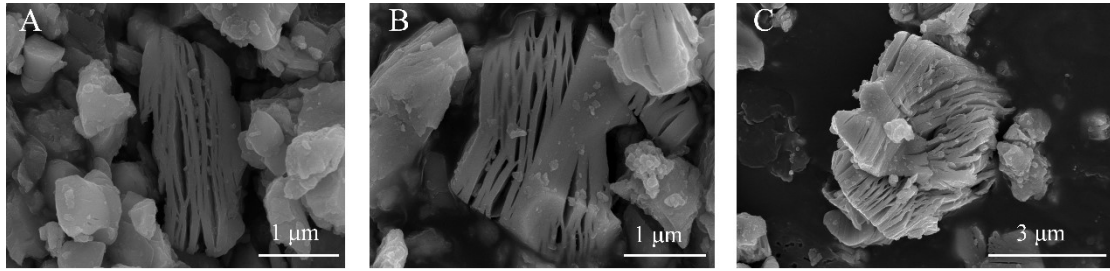


Fig. S1. The effect comparison of different etching times on the morphology of Nb₂CT_x MXene. The etching time was 24 h (A), 36 h (B), and 48 h (C), respectively. From the morphology observation, it was found that Nb₂CT_x MXene with an etching time of 48 hours had better layering effect.

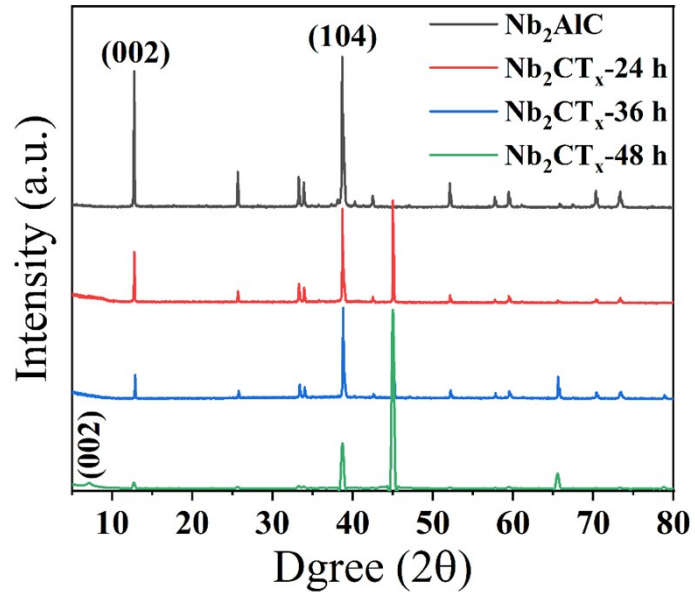


Fig. S2. The effect comparison of different etching times on the crystal form of Nb₂CT_x MXene. It could be seen that after acid etching treatment with 48 h, a new diffraction peak located at $2\theta = 7.1^\circ$ appears and the main peak representing the Al layer (104) is significantly shortened. This proves that the result is better when the etching time is 48 h.

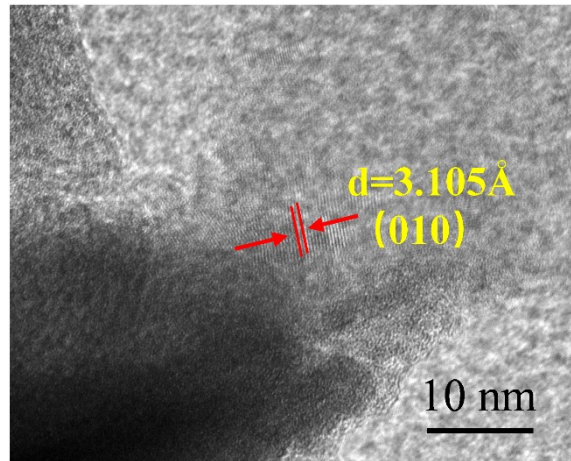


Fig. S3. HRTEM image of petal-like Nb₂CT_x MXene.

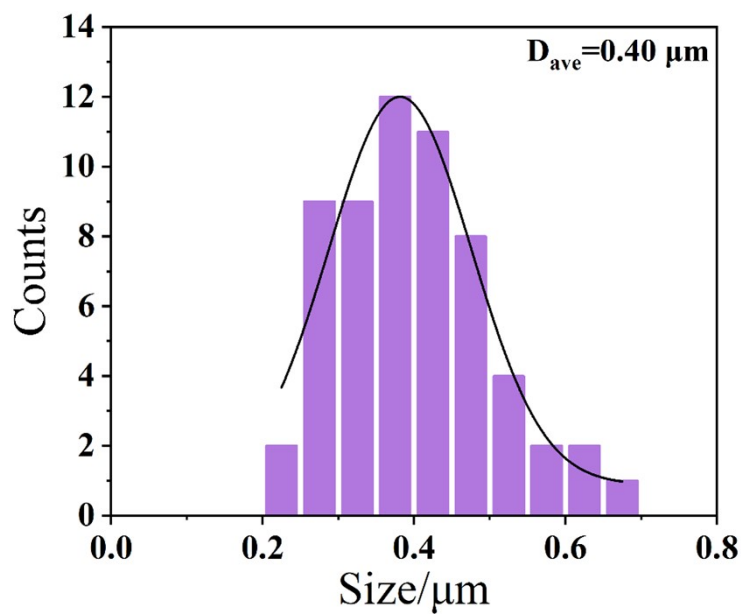


Fig. S4. Statistical analyses of the lateral size of CuNi-MOFs@MQDs in the SEM image.

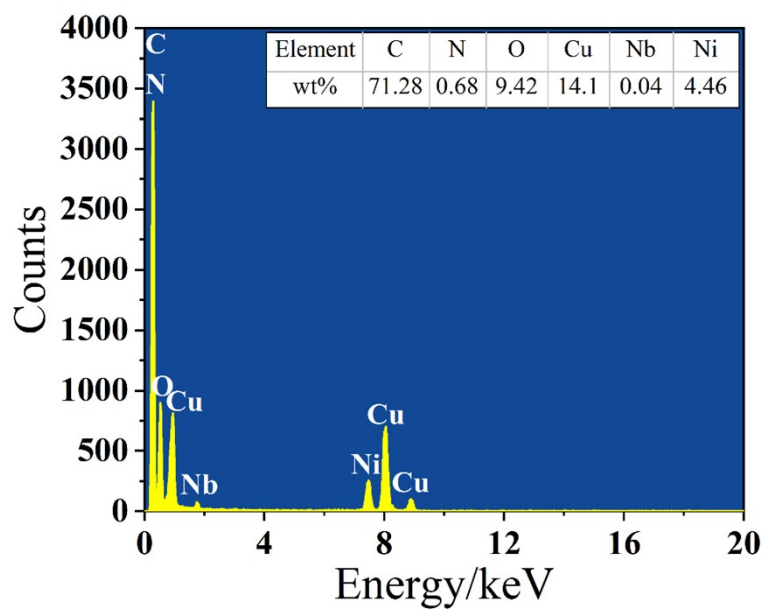


Fig. S5. EDX analysis of CuNi-MOFs@MQDs.

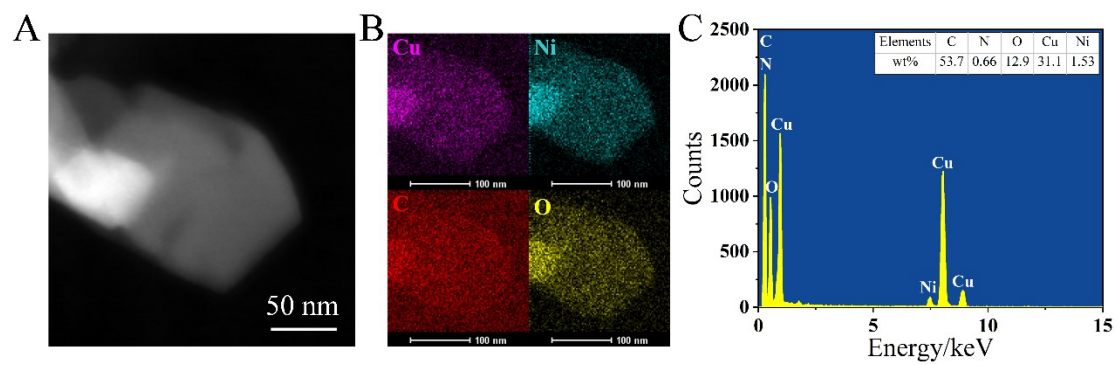


Fig. S6. HAADF images (A), EDX single element distribution (B and C) and EDX analysis of CuNi-MOFs.

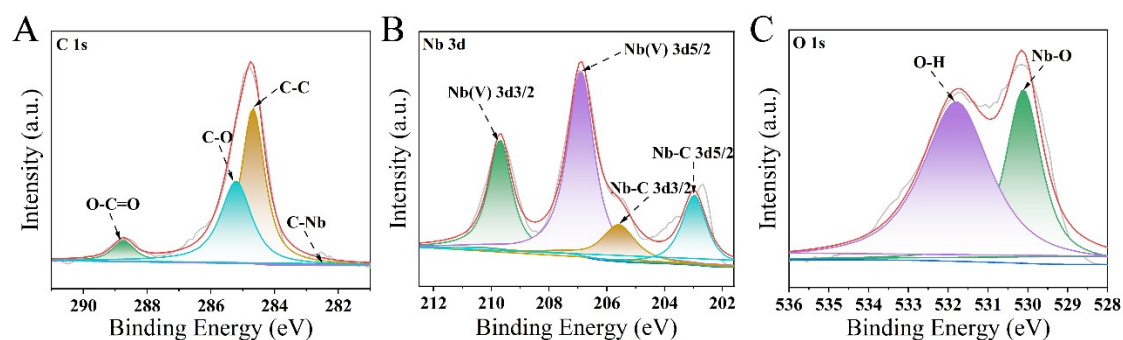


Fig. S7. XPS spectra of Nb₂AlC MAX. High resolution of XPS spectra of C 1s (A), Nb 3d (B), and O 1s (C). The C 1s spectrum (Fig. S7A) shows four peaks located at 288.7 eV, 285.2 eV, 284.6 eV, and 282.5 eV attributed to the O-C=O, C-O, C-C and C-Nb bonds, respectively. Fig. S7c shows the Nb 3d spectrum of Nb₂AlC MAX, the high-resolution Nb 3d spectra were composed of Nb(V) 3d_{3/2}, Nb(V) 3d_{5/2}, Nb-C 3d_{3/2}, and Nb-C 3d_{5/2} at binding energies of 209.6 eV, 206.8 eV, 205.5 eV, and 202.9 eV, respectively. And the O 1s region was composed of O-H (531.8 eV) and Nb-O (530.1 eV).

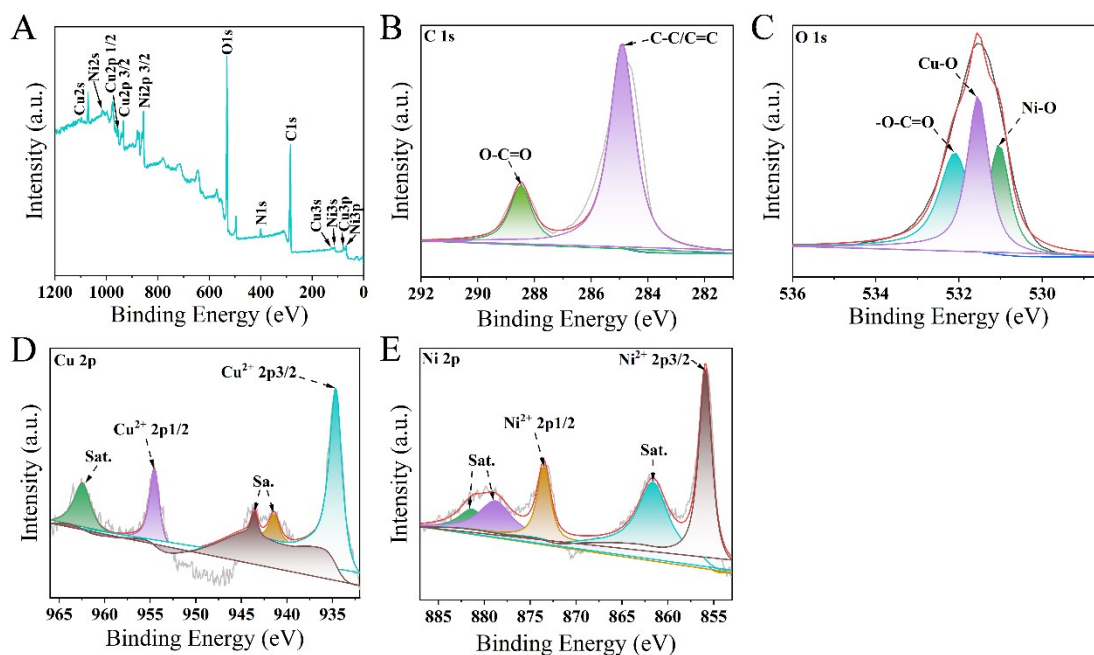


Fig. S8. XPS scan of (A) wide scan of CuNi-MOFs, and high resolution of XPS spectra of C 1s (B), O 1s (C), Cu 2p (D), and Ni 2p (E). The XPS analysis results (Fig. 3C) indicate that the CuNi-MOFs are mainly composed of C, O, Cu, and Ni. The C 1s spectrum (Fig. S8B) shows two peaks located at 288.5 eV and 284.8 eV attributed to the O-C=O and C-C/C=C bonds, respectively. As presented in Fig. S8C, the O 1s region is composed of -O-C=O (532 eV), Cu-O (531.5 eV) and Ni-O (531 eV). In XPS map of Cu 2p (Fig. S8D), the peaks at 934.7 eV and 954.6 eV are Cu^{2+} 2p_{3/2} and Cu^{2+} 2p_{1/2}, respectively. Similarly, in the Ni 2p XPS spectra (Fig. S8E), two main peaks indexing to Ni^{2+} 2p_{3/2} (873.5 eV), and Ni^{2+} 2p_{1/2} (855.9 eV), respectively.

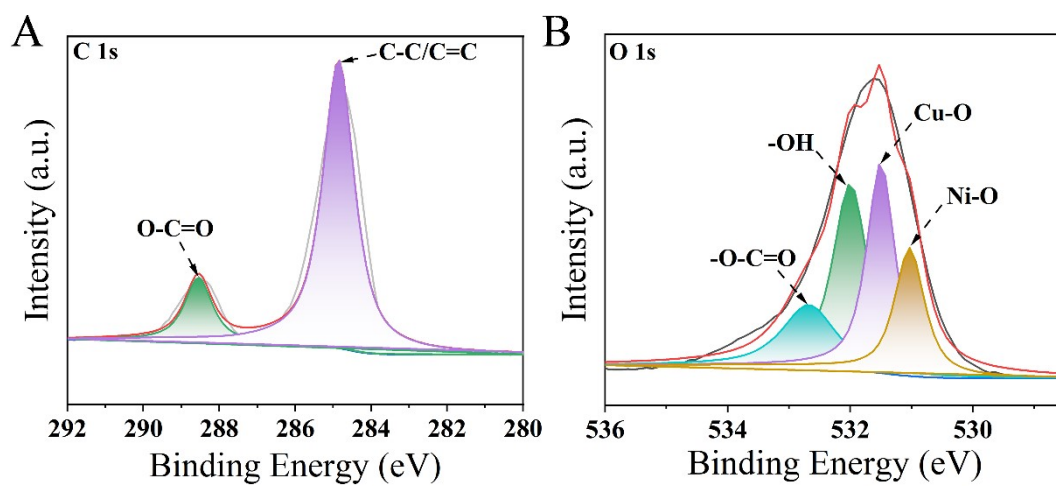


Fig. S9. XPS spectrum of C 1s (A) and O 1s (B) of CuNi-MOFs@MQDs. The C 1s spectrum shows two peaks located at 288.6 eV and 284.8 eV attributed to the O-C=O and C-C/C=C bonds, respectively.

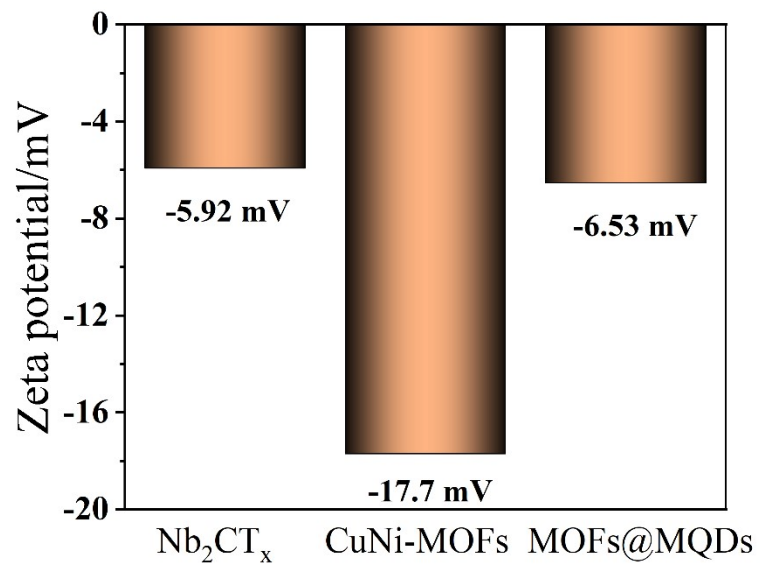


Fig. S10. Zeta potential of Nb₂CT_x, CuNi-MOFs, and CuNi-MOFs@MQDs.

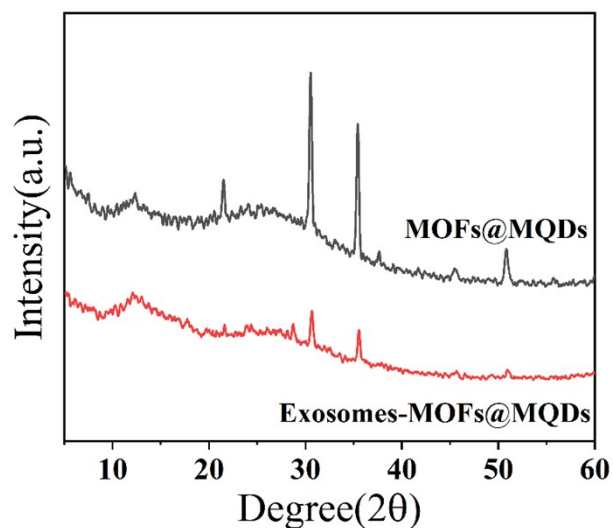


Fig. S11. The XRD spectral results of MOFs@MQDs and exosomes-MOFs@MQDs after 50 CV cycle tests. From the XRD spectrum, it could be seen that after 50 cycles of CV and detection of exosomes, the diffraction peak position of the composite material did not shift, indicating that the crystal structure did not change. However, the intensity of the characteristic peak decreases, which means that the crystallinity of the material has decreased.

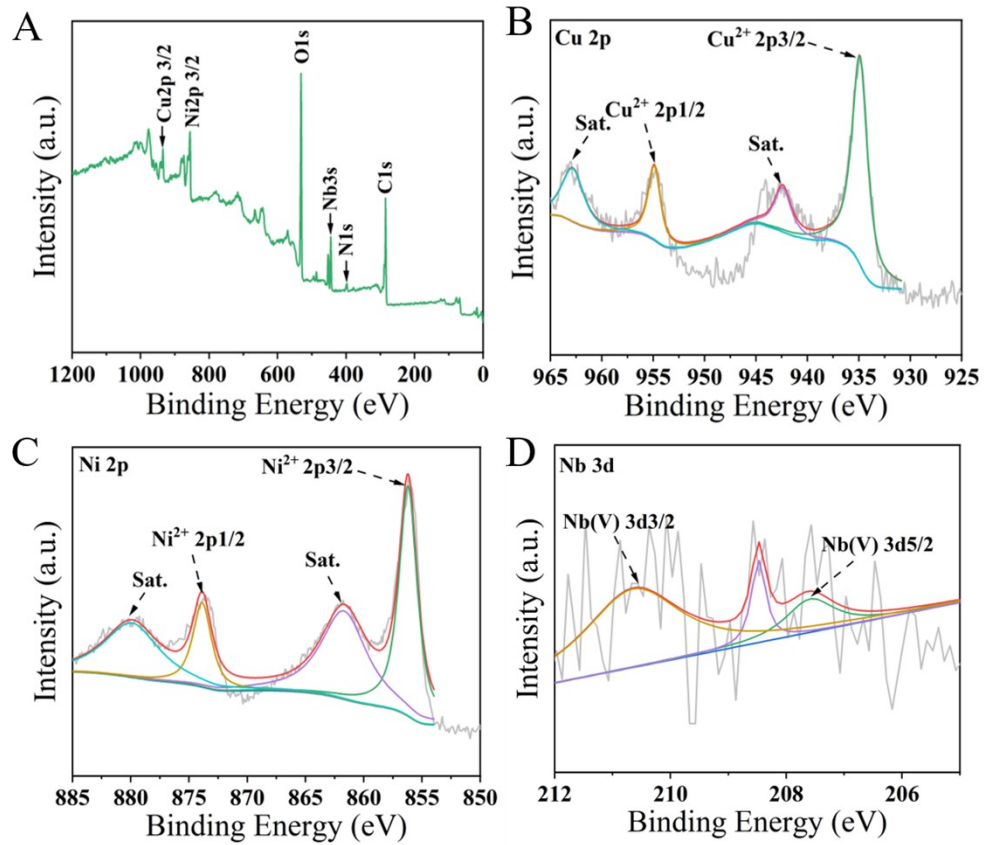


Fig. S12. The XPS spectral of MOFs@MQDs after 50 CV cycle tests.

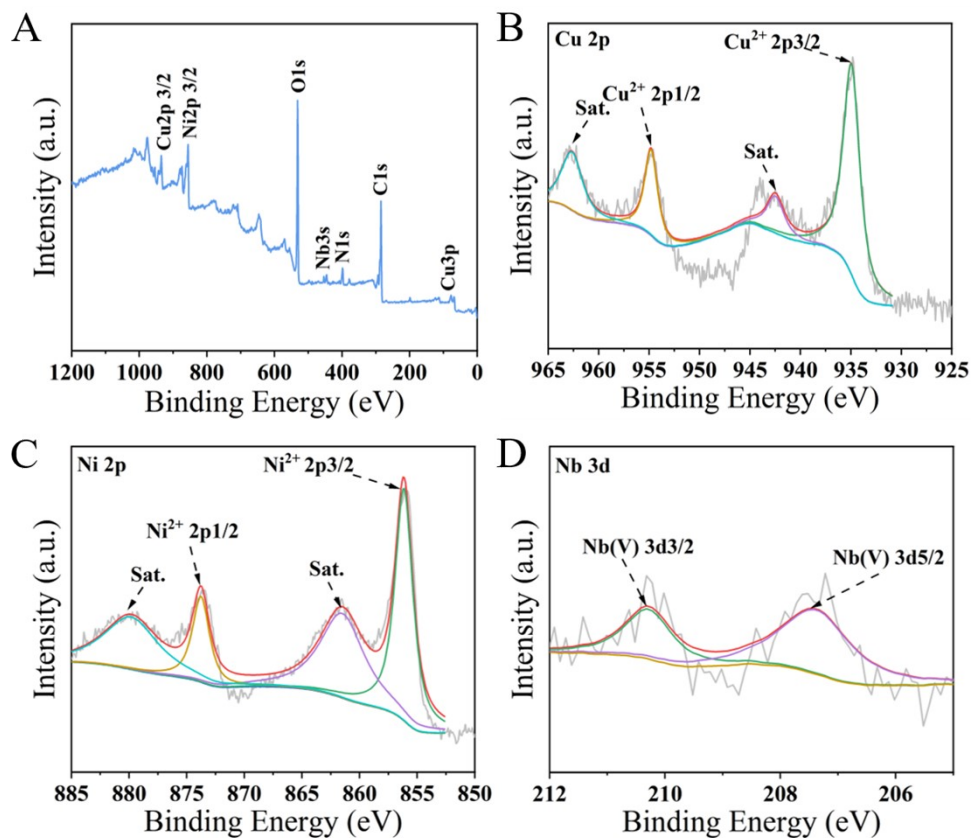


Fig. S13. The XPS spectral of exosomes-MOFs@MQDs after 50 CV cycle tests. The material was characterized by XPS after long-term CV cycling, and the peak area was calculated. It was found that the peak area of Cu^{2+} , Ni^{2+} , and Nb (V) decreased after long-term cycling, indicating that the reduction reaction of Cu^{2+} , Ni^{2+} , and Nb (V) may have occurred during the electrochemical sensing process, thus achieving detection and sensing.

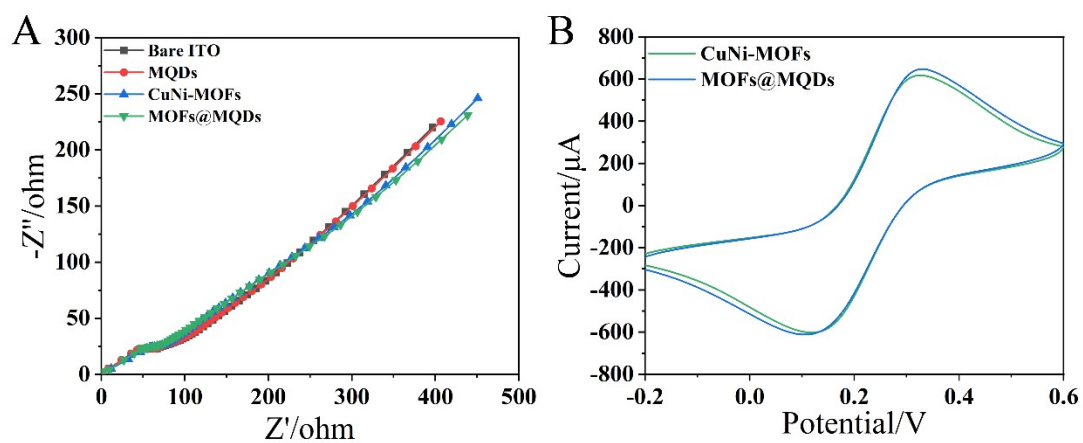


Fig. S14. EIS graphs (A) of different modified electrodes and CV curves (B) of CuNi-MOFs and CuNi-MOFs@MQDs. The semi-circle of the high frequency region of the EIS spectrum represents the electron transfer limitation process, and the linear part of the low frequency region corresponds to the diffusion limitation process. As can be seen from the figure, MOFs@MQDs has the smallest semi-circle in the high frequency region, where the electron transfer rate of the substrate surface is the fastest and the impedance is the smallest, indicating that the combination of MOFs and MQDs improve the electrochemical conductivity. And the EIS results corresponds to the CV results in Fig.S11B.

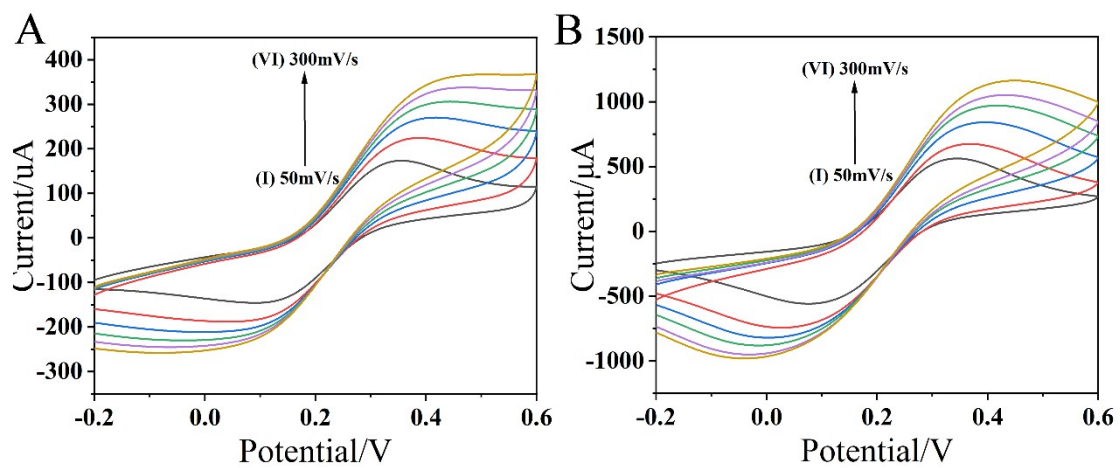


Fig. S15. CV curves of (A) bare ITO electrode and (B) MQDs-based electrode at different scan rates from 50 mV/s to 300 mV/s. The system of CV contains 5 mM $\text{K}_3[\text{Fe}(\text{CN})_6]$ and 0.1 M KCl.

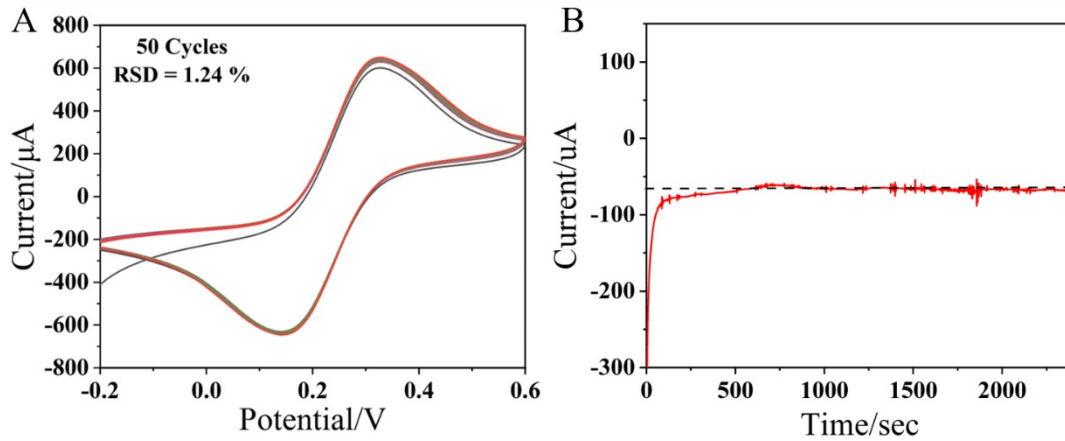


Fig. S16. The CV tests (A) and Amperometric *i-t* curves (B) of MQDs. As shown in the figure below, the long cycling performance of MQDs was first tested by CV. It could be seen that the peak current of oxidation and reduction changes slightly, and RSD is 1.24%, indicating excellent cycle performance. In addition, the stability of the MQDs sensor was tested using the Amperometric *i-t* method, and within 2400 s, the current remained basically stable without significant deviation, indicating that it has good stability. Therefore, the MQDs tested in the article have good performance.

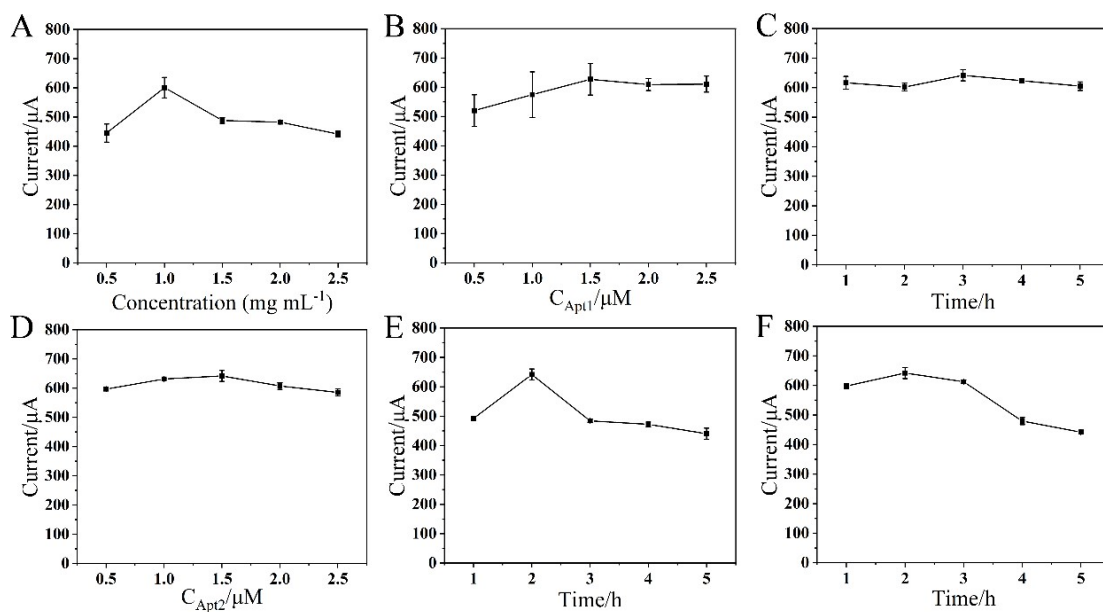


Fig. S17. The effect of different parameters on the sensing performance of the as-prepared aptasensor by DPV responses. (A) The concentrations of CuNi-MOFs@MQDs, (B) The concentrations of Apt1, (C) The incubation time of Apt1, (D) The concentrations of Apt2, (E) The incubation time of Apt2, and (F) The incubation time of exosomes. The concentration of exosomes is 1×10^3 particles μL^{-1} .

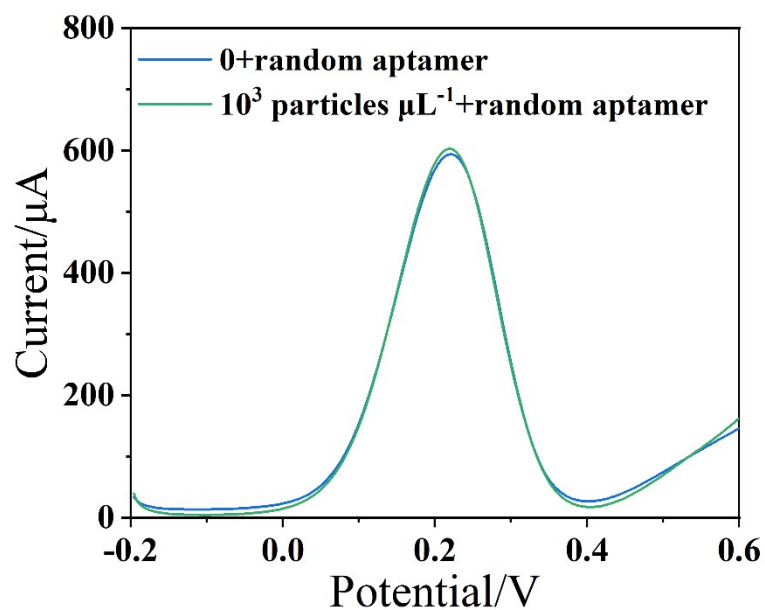


Fig. S18. DPV responses before and after detecting exosomes using sensors connected to the random aptamer. The concentration of exosomes is 1×10^3 particles μL^{-1} . There is no significant change in the electrochemical signal between the sensor connected to the random aptamer and the sensor not connected to the aptamer, indicating that the random aptamer can not achieve the detection of exosomes.

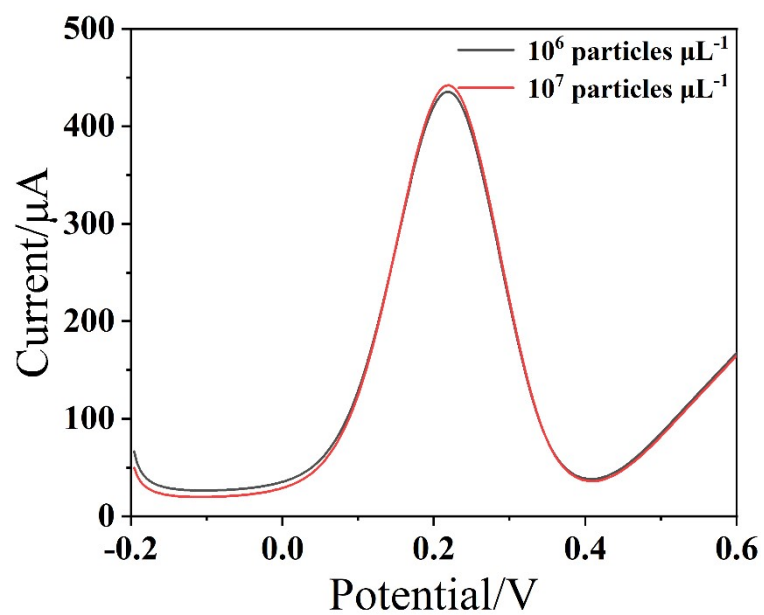


Fig. S19. The DPV responses were obtained after incubating 500 μL of exosomes with concentration of 1×10^6 and 1×10^7 particles μL^{-1} with the constructed aptasensor. It could be observed that increasing the concentration of exosomes does not result in a gradient increase in the electrochemical signal, indicating that the maximum detection limit of the aptasensor is 1×10^6 particles μL^{-1} .

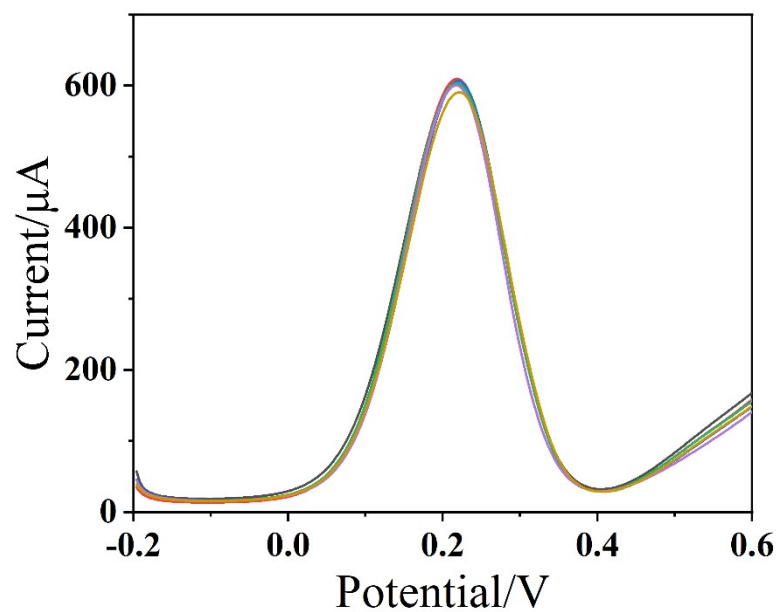


Fig. S20. The DPV current of 6 parallel tests with exosomes. The concentration of exosomes was 1×10^3 particles μL^{-1} . From the result graph, it could be seen that there was not much difference in electrochemical signals when detecting the same concentration of exosomes, indicating that the prepared aptasensor has good detection stability.

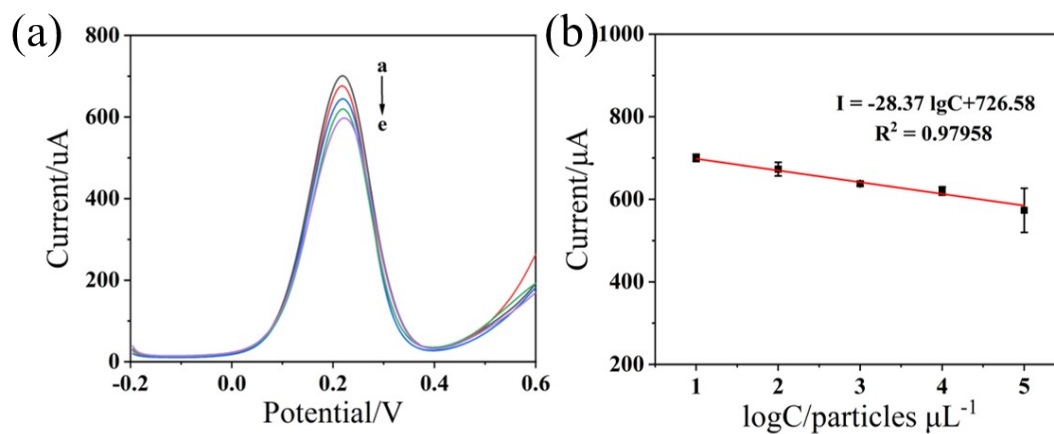


Fig. S21. (A) DPV responses of the Apt1/CuNi-MOFs@MQDs/ITO at different concentrations of exosomes (particles μL^{-1}) from a to e: 1×10^1 , 1×10^2 , 1×10^3 , 1×10^4 , and 1×10^5 . (B) Calibration plot of the aptasensor for exosomes detection with a coefficient of determination ($R^2 = 0.97958$). The LOD of the Apt1/CuNi-MOFs@MQDs/ITO sensor was obtained as 6 particles μL^{-1} ($S/N=3$).

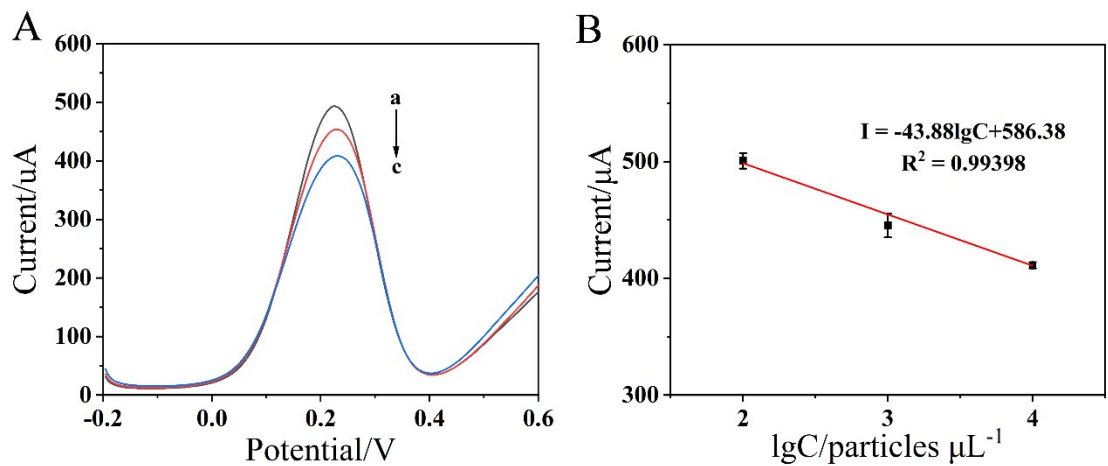


Fig. S22. (A) DPV responses of the Apt2/CuNi-MOFs@MQDs/ITO at different concentrations of exosomes (particles μL^{-1}) from a to c: 1×10^1 , 1×10^2 , and 1×10^3 . (B) Calibration plot of the aptasensor for exosomes detection with a coefficient of determination ($R^2 = 0.99398$). The LOD of the Apt2/CuNi-MOFs@MQDs/ITO sensor was obtained as $71 \text{ particles } \mu\text{L}^{-1}$ ($S/N=3$).

Table S1. Comparison of the detection performance for the exosomes with other electrochemical sensors.

Modification Material	Detection method	Linear range (particles μL^{-1})	Detection limit (particles μL^{-1})	Ref
HRP-pSC ₄ -AuNPs@COFs	Amperometric	$5 \times 10^2 - 5 \times 10^7$	1.6×10^2	1
Cucurbit [7] uril and ferrocene	DPV	$5 \times 10^2 - 5 \times 10^3$	4.82×10^2	2
C60-Au-Tb composite	SWV	$5 \times 10^1 - 5 \times 10^6$	2.67×10^1	3
DNA/SWCNT-Fc	SWV	$4.66 \times 10^3 - 9.32 \times 10^6$	9.38×10^1	4
PB-MXene	SWV	$5 \times 10^2 - 5 \times 10^5$	2.29×10^2	5
AuNPs@MCF/MWCNTs	DPV	$1 \times 10^2 - 1 \times 10^7$	7×10^1	6
Histostar@COFs	Amperometric	$1 \times 10^3 - 1 \times 10^8$	3.18×10^2	7
Zr-MOFs	SWV	$9.5 \times 10^3 - 1.9 \times 10^7$	7.83×10^3	8
CuNi-MOFs@MQDs	DPV	$1 \times 10^1 - 1 \times 10^6$	5	This work

References

1. M. Wang, Y. Pan, S. Wu, Z. Sun, L. Wang, J. Yang, Y. Yin and G. Li, *Biosens Bioelectron*, 2020, **169**, 112638.
2. Q. Liu, X. Yue, Y. Li, F. Wu, M. Meng, Y. Yin and R. Xi, *Talanta*, 2021, **232**, 122451.
3. Z. Liu, H. Wang, J. Li, M. Wang, H. Yang, F. Si and J. Kong, *Microchem J*, 2021, **170**, 106772.
4. F. Si, Z. Liu, J. Li, H. Yang, Y. Liu and J. Kong, *Anal Biochem*, 2023, **660**, 114971.
5. H. Zhang, Z. Wang, F. Wang, Y. Zhang, H. Wang and Y. Liu, *Talanta*, 2021, **224**, 121879.
6. N. Sahraei, M. Mazloum-Ardakani, A. Khoshroo, F. Hoseynidokht, J. Mohiti and A. Moradi, *J Electroanal Chem*, 2022, **920**, 116590.
7. Y. Lin, B. Nie, X. Qu, M. Wang, J. Yang and G. Li, *Biosensors (Basel)*, 2022, **12**.
8. Z. Sun, L. Wang, S. Wu, Y. Pan, Y. Dong, S. Zhu, J. Yang, Y. Yin and G. Li, *Anal Chem*, 2020, **92**, 3819-3826.